

Design of a self-adaptive oscillating neuron using an electrically reconfigurable skyrmion lattice

Priyamvada Jadaun*, Can Cui and Jean Anne C. Incorvia

Dept. of Electrical and Computer Engineering, The University of Texas at Austin

(Dated: December 22, 2020)

*priyamvada@utexas.edu

ABSTRACT

Artificial Intelligence (AI) promises to fundamentally transform society; however, the realization of this potential faces multiple challenges, as state-of-the-art AI is energy-intensive and lacks the advanced cognitive capabilities of the brain. While spintronic neuromorphic computing can enable the implementation of ultra-low-power AI, cutting-edge spintronic neuromorphic devices have yet to realize many advanced neural properties. Here, we design and simulate the dynamics of a self-adaptive spintronic artificial neuron that incorporates two advanced neuronal properties: neural oscillation and neuromodulation. The proposed neuron utilizes the coupled oscillatory dynamics of five magnetic skyrmions hosted in a bilayer of thulium iron garnet (TmIG) and platinum (Pt). Micromagnetic simulations show that the neuron has four distinct resonant modes that are identified as skyrmion gyration, breathing, and the hybridizations of both. Both the amplitudes and frequencies of these modes can be modified by reconfiguring the skyrmion lattice, thereby emulating neuromodulation. The multi-frequency resonant spectrum of the neuron provides a large, flexible basis for information encoding. Utilizing these advanced neuronal dynamics, we demonstrate bio-plausible neuronal functions such as cross-frequency coupling and bursting, and advanced cognitive processes such as context-awareness and feature binding. Context awareness is implemented for a task in which a robot decides whether to open a box, given a human spoken command and contextual information about the color of the box. Feature binding is realized for a task where a neural network combines different segments of information regarding the shape and color of an object, to construct a coherent percept of the perceived object. Building context-awareness and feature binding into AI can fundamentally transform a wide array of fields including personalized medicine, neuro-prosthesis, human-machine interaction and industrial manufacturing. The advanced cognitive abilities of the self-adaptive neuron thus provide a path for the next generation of context-aware AI, one that understands and adapts to a complex and dynamic environment, learns without supervision from small datasets and better collaborates with human beings.

INTRODUCTION

Recent years have witnessed an explosive growth in artificial intelligence (AI) that excels at big-data applications such as language translation, virtual assistants and bioinformatics [1, 2, 3]. However, state-of-the-art AI lacks the advanced cognitive abilities displayed by the brain, including the ability to adapt to its environment, to understand context and to integrate various segments of information into a coherent representation of the external world. The realization of AI with these advanced properties can transform virtually every sector of society [4, 5]. Moreover, state-of-the-art AI when implemented with conventional CMOS uses significant energy and area [6].

Inspired by the brain, neuromorphic computing can achieve an ultra-low-power implementation of AI [7, 8, 9]. Spintronic nanodevices are particularly attractive for neuromorphic hardware, owing to their small footprint, high endurance and low power consumption [10, 11]. In particular, topologically-stable chiral magnetic states (skyrmions) are beneficial due to their small size and their ability to be created, manipulated, detected and erased by current or field [12]. Moreover, skyrmion-skyrmion coupling [13, 14] can produce a multi-frequent spectrum for information encoding. However, cutting-edge neuromorphic devices still largely mimic simple neuronal properties like spiking [15, 16], whereas biological neurons demonstrate more rich, adaptive and computationally powerful behavior such as neural oscillations and neuromodulation [17, 18, 19].

Neural oscillations are rhythmic activities in the brain that occur at all levels of neural organization [19]. At the same time, neuromodulation is a mechanism by which the brain regulates its functioning in real-time. Neuromodulation alters the amplitude and frequency of oscillations in neural circuits, enabling the brain's impressive ability to adapt to its surroundings [20, 17]. Both oscillations and neuromodulation are shown to play a critical role in advanced cognitive processes, including information transfer and decision-making [21], memory [22], object representation [23, 24, 25], visual perception [26, 27], attention [23, 28] and consciousness [22].

While research on neuromorphic computing has seen significant advancement, neuromorphic implementation of neural oscillations has been very limited [29, 30] and neuromodulation of these oscillations has yet to be achieved. Moreover, state-of-the-art spintronic oscillating neurons exhibit simple oscillatory dynamics with one resonant frequency [31, 32, 33], and have not yet emulated the multi-frequency spectra displayed by the brain in EEG recordings [34]. Similarly, skyrmions have only been designed as the simple spiking neurons mentioned above [35, 36, 37].

Here, we design and simulate a self-adaptive artificial neuron named Tunable-SKYrmion-based Oscillating NEuron (T-SKONE) that incorporates both neural oscillations and neuromodulation, and we utilize it to pioneer the realization of two advanced cognitive processes: context-awareness and feature binding. The self-adaptive neuron consists of an artificial skyrmion lattice with five

skyrmions hosted in a bilayer of insulating thulium iron garnet (TmIG) and platinum (Pt). Simulations performed with MuMax3 micromagnetic modeling show that when excited by an oscillating magnetic field, the neuron produces spin waves originating from skyrmion oscillations that demonstrate a multi-frequency spectrum. The spectrum consists of four distinct resonant modes, identified as counterclockwise (CCW) gyration, breathing, and the hybridizations of both. Since each resonant frequency can represent one bit of information, the multi-frequent spectrum provides a large basis of information representation [32]. Moreover, we demonstrate that both the amplitude and frequency of these resonant modes can be modulated by re-arranging the skyrmions in the lattice, thereby emulating neuromodulation.

T-SKONE is further utilized to implement complex neuronal dynamics such as bursting and cross-frequency coupling [22], as well as advanced cognitive processes, namely context-awareness and feature binding. Context-awareness allows the neuron to make complex, high-level decisions while taking into account multiple factors, developing a deeper understanding of its circumstance. To implement context-awareness, T-SKONE receives a human spoken command and contextual information about the color of a box. Integrating both inputs, the neuron decides to open the box if and only if the human being gives the direction to open and the box is not red in color. In addition, feature binding allows the neuron to correctly combine different segments of information (say, color = ‘red’ and shape = ‘circle’) and construct a coherent percept (object = ‘red circle’). To implement feature binding, a network of T-SKONEs receives visual information about two objects, a ‘red circle’ and a ‘blue cross’. The network processes information about the shape and color of the objects separately, and then correctly binds together the two features to obtain coherent percepts of the original object. Taking inspiration from the brain, we achieve feature binding with the help of phase-coding. A large body of work suggests that in the brain, the phase of a low-frequency oscillation (gamma wave) helps to bind the various features of an object by having the relevant neuronal ensembles oscillate rhythmically together at the same frequency [38, 39, 40, 41, 42, 43]. Analogously, various features of the same object are encoded by T-SKONE using the same modulatory phase, and therefore at the same frequency, which allow the features to be correctly integrated via synchronization [44, 45, 46, 47, 48].

These results realize context-aware AI which can have sweeping impact on human-machine collaboration, personalized healthcare, advanced manufacturing and education [5, 49, 50, 51]. Additionally, the work enables feature binding or fusion of information from different sensory streams which can fundamentally transform autonomous vehicles, neuro-prosthesis, wearable health technology, agriculture and climate control [52, 53, 54, 55]. Moreover, our implementation of phase-coding actualizes synchronization based dynamic coupling in neuromorphic circuits making them adaptive, fast and flexible [56, 22, 24]. Therefore, the self-adaptive neuron, and more generally, neuromorphic devices with advanced cognitive abilities can usher in the next wave of AI, one that understands and adapts to a complex and dynamic environment, learns without supervision from small datasets and better collaborates with human beings [4, 57].

RESULTS

NEURON DESIGN AND FUNCTION - A schematic of T-SKONE is shown in Fig. 1 (a). The skyrmion lattice comprises five nanotracks, (with a nanotrack along y) each hosting a single skyrmion (blue). The five skyrmions are labeled $Sk1 - Sk5$ along increasing x , as shown in Fig. 1 (b). To precisely arrange the skyrmions in the lattice and prevent skyrmion dislocation upon application of an oscillatory magnetic field, reduced perpendicular magnetic anisotropy (PMA) regions are used as skyrmion pinning sites (shadowed regions in Fig. 1 (b)). Such reduced PMA regions can be created using ion implantation [58]. Since the skyrmion boundary with in-plane magnetization tends to be located in the low-PMA regions to reduce the overall magnetostatic energy [59], the skyrmions can be softly pinned into lattice sites A or B (Fig. 1 (b)). The neuron receives two types of inputs: (i) a global, excitatory magnetic field input (H_{RF}) along x applied to all skyrmions through a gold strip line antenna, which induces localized skyrmion oscillations and produces spin waves [60, 61], and (ii) local, modulatory current inputs ($J_1 - J_5$) along y applied to individual skyrmions through the spin Hall metal Pt overlayers (purple), which independently move the skyrmions along the nanotracks and position them in site A or B. As the skyrmion lattice configuration is modified (e.g. between Configurations I and II as shown in Fig. 1 (b)), so are the skyrmion coupling strengths and therefore their resonant frequencies and amplitudes of oscillation. Thus, the response of the neuron to the excitatory input can be controlled by the modulatory currents, mimicking neuromodulation. The outputs from the skyrmion nanotracks are carried by co-planar waveguides composed of an insulating magnet (YIG) to be subsequently processed and combined.

Recent work has reported the observation of above and near room-temperature skyrmions in a bilayer heterostructure composed of a magnetic insulator, thulium iron garnet (TmIG, $Tm_3Fe_5O_{12}$) in contact with a spin Hall metal (Pt) [62]. There have also been experimental observations of domain wall motion in TmIG/Pt bilayers driven by spin orbit torque [63] [64]. The TmIG/Pt system provides innate electrical isolation to the individual nanotracks, while at the same time allowing the skyrmions to couple magnetically. However, since the skyrmion phase in TmIG/Pt typically exists at and above 360 K, more work is required for the design of room-temperature stable insulating skyrmion materials.

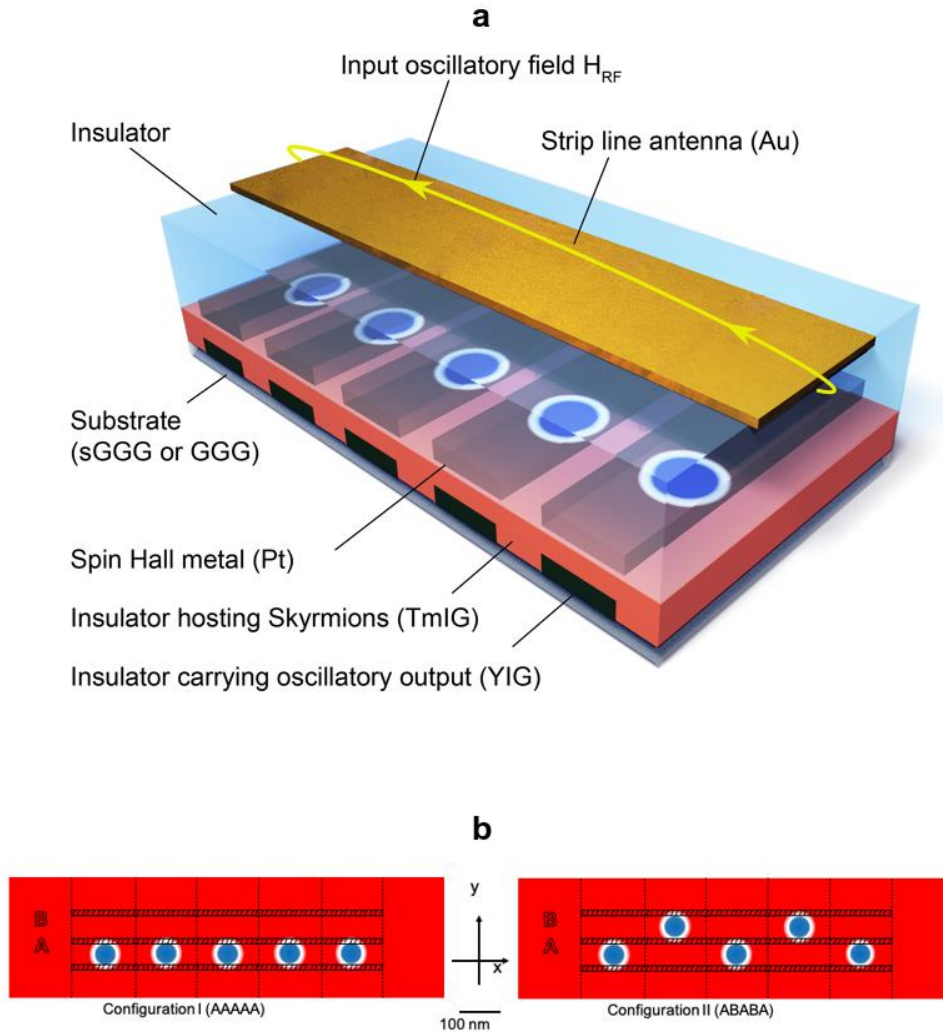


FIG. 1. Schematic of the self-adaptive oscillating neuron. (a) Structure of the neuron. TmIG (salmon): insulating magnet hosting the skyrmion lattice. H_{RF} : excitatory magnetic field input carried by the strip line antenna. $J_1 - J_5$: modulatory current inputs carried by the spin Hall metal (Pt). YIG: spin waves output readout. (b) Top-down views of the skyrmion lattice, with skyrmions (blue) arranged in Configuration I (AAAAA, left) and II (ABABA, right), respectively. The shadowed regions have reduced perpendicular magnetic anisotropy, designed to softly pin the skyrmions.

NEURONAL DYNAMICS - The oscillatory dynamics of T-SKONE was simulated for two lattice configurations, Configuration I (AAAAA) and II (ABABA), using the MuMax3 solver [65], as described in Methods. The fast Fourier transform (FFT) power density spectra of the skyrmion

core trajectories was calculated (see Methods) and is shown in Fig. 2 (a-b), with Configuration I in solid blue and Configuration II in dashed magenta. As the configuration of the neuron changes, the peaks of the spectrum that signify the resonant frequencies also shift, which demonstrates that the neuron is capable of Frequency Modulation. Figure 2 (a) shows two resonant peaks for both configurations at around 0.80 GHz and 1.04 GHz corresponding to Mode 1 and Mode 2, respectively. The FFT spectra when zoomed-in and extended up to 2.0 GHz is shown in Fig. 2 (b), where two more resonant peaks around 1.22 GHz (Mode 3) and around 1.85 GHz (Mode 4) can be seen. We note here there are at least 8 different neuronal configurations available in this design.

To demonstrate Amplitude Modulation, the neuron was excited by a sinusoidal magnetic field as described in Methods. Figure 2 (c-f) show the amplitudes of oscillations of the skyrmion cores along x at driving frequency ranges centered on (c) Mode 1, (d) Mode 2, (e) Mode 3, and (f) Mode 4. There are multiple instances of a clear difference in the amplitudes of oscillations at a given frequency for Configurations I (solid blue) and II (dashed magenta), which demonstrates Amplitude Modulation. For instance, at 0.80 GHz (Mode 1) $Sk3$ has a larger amplitude of oscillation for Configuration II than I, while $Sk5$ shows a larger amplitude for Configuration I than II, both of which are consistent with the FFT power spectrum. It is worth noting that the small driving field (10 Oe) required to induce large oscillation amplitudes (up to 8 nm) is highly promising for ultra-low power operation of the neuron. Amplitude Modulation along y is shown in Supplementary Information S1.

We now discuss the four resonant modes identified above in more detail. Figure 3 shows the oscillatory response of the neuron while in Configuration I, upon excitation with a sinusoidal magnetic field. The first and second columns of Fig. 3 (a-d) plot the oscillations for every skyrmion core along x and y , respectively, for resonant modes (1-4). The skyrmion cores oscillate sinusoidally with frequencies locked to the driving input and with a wide range of amplitudes. To reveal the physical origin of these modes, topological charge density maps of the T-SKONE are plotted at times $t = 0, T/4, T/2$ and $3T/4$, where T is the respective time period of oscillation. These maps are shown in the four columns on the right of Fig. 3 and demonstrate that every resonant mode originates from a distinct type of skyrmion dynamics. In general, the oscillation amplitudes are larger for the outer skyrmions ($Sk1$ and $Sk5$) than amplitudes for inner skyrmions ($Sk2 - Sk4$). This is likely because the dominant form of interaction is the skyrmion-skyrmion repulsion which suppresses the oscillations of the inner skyrmions.

Figure 3 (a) shows the skyrmion oscillation for Configuration I at Mode 1 (0.80 GHz). The topological charge density plots demonstrate that this is a breathing mode, in which the skyrmions periodically expand and contract in size. At this frequency the skyrmions are out-of-phase with their neighbors, which is favored by the skyrmion-skyrmion repulsion. Figure 3 (b) plots the output for Configuration I at Mode 2 (1.04 GHz). From the topological charge density maps, a mixture of the two oscillations instead of complete cycles of breathing mode or gyration mode are observed

over the time period of oscillation, which indicates that this mode is a hybridization between these two pure modes. The amplitudes for the inner skyrmions ($Sk_2 - Sk_4$) are comparable, and their oscillations while not perfectly phase-locked are similar in their phase ordering. This is expected due to the hybridized nature of Mode 2.

Skyrmion oscillations at Mode 3 (1.22 GHz) are shown in Fig. 3 (c). Topological charge density plots reveal the origin of this mode to be a CCW gyration mode with all the skyrmions synchronized at 1.22 GHz. Finally, Fig. 3 (d) demonstrates oscillatory dynamics at Mode 4 (1.85 GHz) where oscillations for all skyrmions are generally small (< 1 nm). Topological charge densities reveal this to be a highly complex mode originating from the hybridization of breathing, counterclockwise and clockwise gyration.

With few exceptions, the largest oscillatory amplitudes were seen for Modes 1 and 3 and the smallest were seen for Mode 4. This is likely because Modes 1 and 3 are pure modes whereas Modes 2 and 4 are hybridizations of the pure modes. The frequency range corresponding to Mode 2 lies between that of the pure Modes 1 and 3, since Mode 2 is a hybridization of Modes 1 and 3. The discovery of hybridized modes in skyrmion lattices brings a particularly rich and coupled dynamics to the oscillatory neuron, enhancing its utility for neuromorphic applications. When the neuron in Configuration II was excited with the same frequencies as above, it also demonstrated four modes with the same physical origin, but with different oscillation amplitudes (see Supplementary Information S2). Additionally, Amplitude Modulation and Frequency Modulation were demonstrated using the metallic CoFeB/heavy metal bilayer system (see Supplementary Information S3).

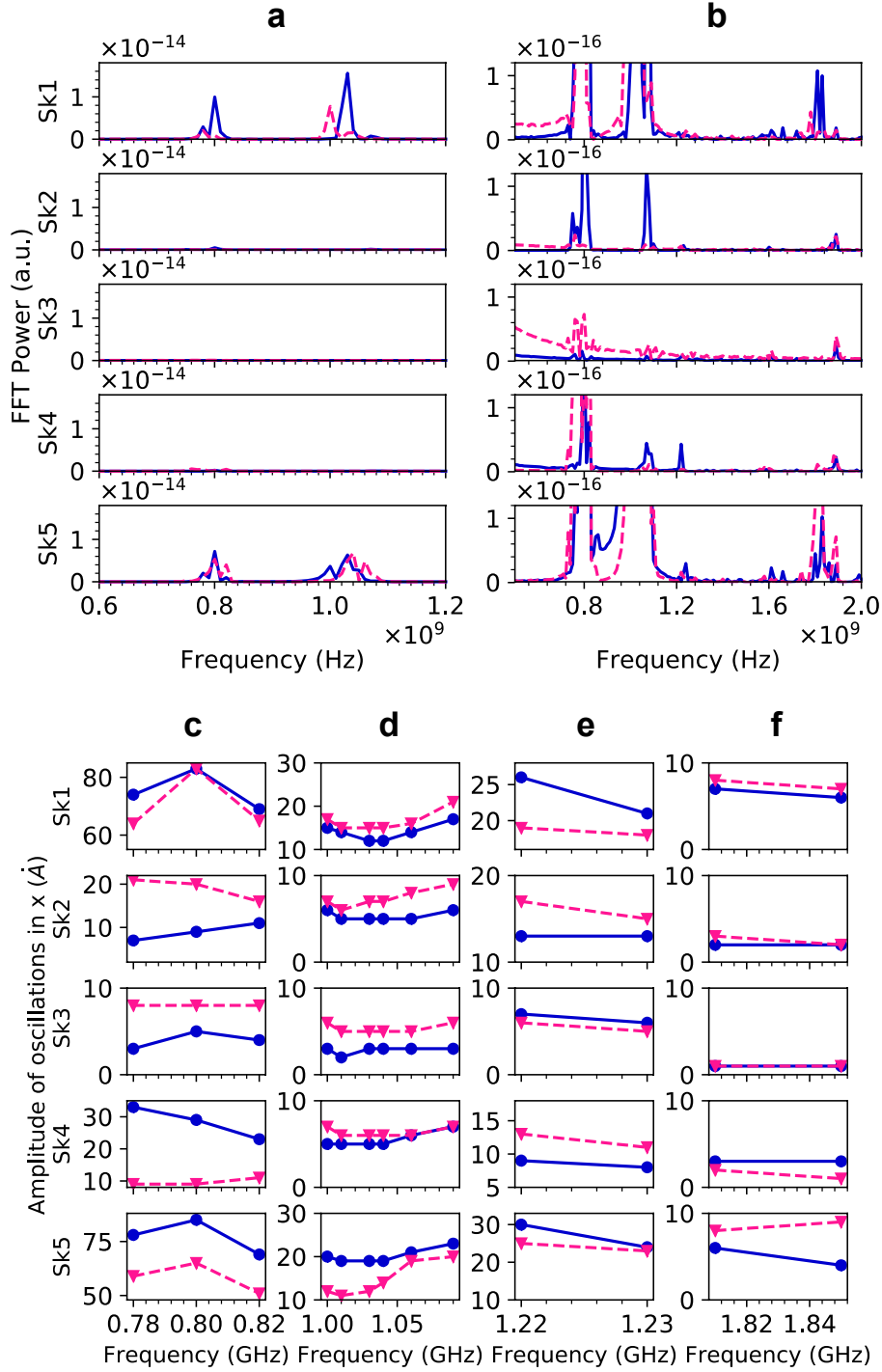


FIG. 2. Coupled dynamics of T-SKONE. (a) Frequency Modulation: Fast Fourier transform (FFT) power density spectra of the neuron for Configuration I (solid blue line) and Configuration II (dashed magenta line), for all five skyrmions ($Sk1 - Sk5$). (b) Zoomed-in plot of (a). (c-f) Amplitude modulation: Amplitudes of oscillation for all five skyrmions shown at a range of frequencies for Configuration I (blue circles) and Configuration II (magenta triangles).

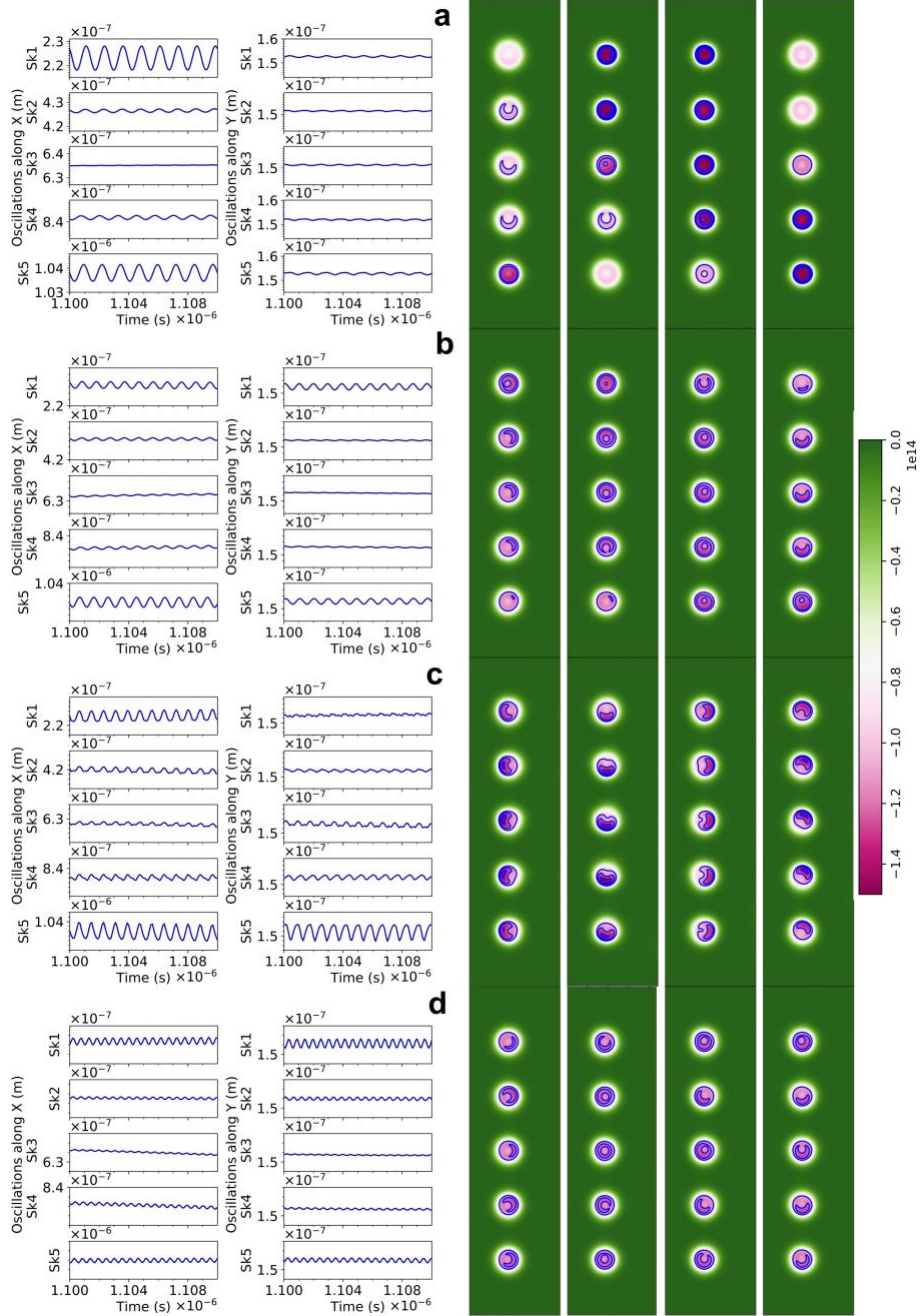


FIG. 3. Resonant modes of T-SKONE in Configuration I when excited by a sinusoidal driving field of frequency (a) 0.80 GHz (Mode 1), (b) 1.04 GHz (Mode 2), (c) 1.22 GHz (Mode 3) and (d) 1.85 GHz (Mode 4). The two left most columns plot the output oscillations along x and y , respectively. The four columns on the right plot the topological charge densities at times $t = 0, T/4, T/2, 3T/4$, where T is the respective time period of oscillation. The color maps for topological charge density ranges from $-1.5 \times 10^{14} m^{-2}$ (magenta) to zero (green).

ADDITIONAL BIO-INSPIRED DYNAMICS BASED ON NEUROMODULATION -

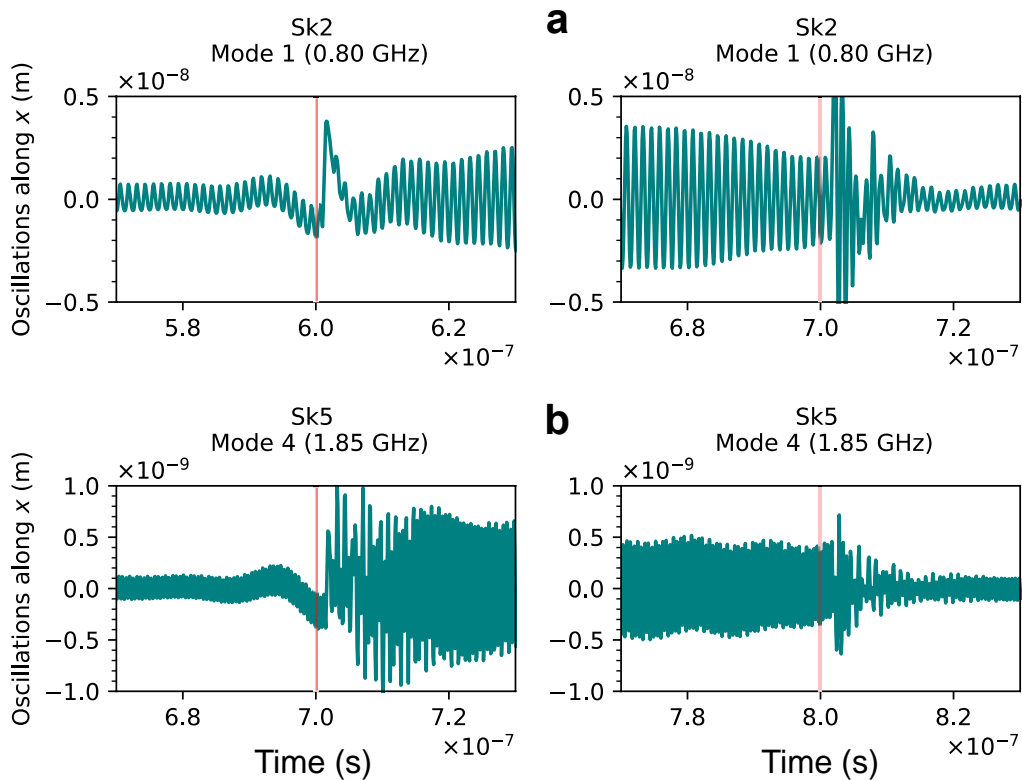


FIG. 4. Bursting dynamics of T-SKONE. The figure plots the oscillatory output of the neuron in real-time, as it is reconfigured from Configuration I to II to I, (a) for a driving frequency of 0.80 GHz and (b) for a driving frequency 1.85 GHz. The neuron, in particular *Sk2* for (a) and *Sk5* for (b), demonstrates bursting properties as it transitions from oscillations with smaller amplitudes to those with larger amplitudes and back. The onset of reconfiguration is marked in red.

To demonstrate that neuromodulation of T-SKONE can lead to cross-frequency coupling [22] and bursting dynamics, the neuron was periodically reconfigured between Configuration I and II by a modulatory input, as it was continuously excited by a sinusoidal magnetic field (see Methods). Figure 4 (a) and (b) plot the output oscillations of *Sk2* and *Sk5* along x , respectively, and clearly demonstrate that the low-frequency modulatory input controls the amplitude of the high-frequency neuronal output, implementing cross-frequency coupling. The dynamics also demonstrate neuronal bursting, where a neuron emits a burst or group of spikes.

NEUROMORPHIC IMPLEMENTATION - We now utilize neuromodulation and the bio-plausible dynamics of T-SKONE for the neuromorphic implementation of two advanced cognitive processes: context-awareness and feature binding.

Context-awareness is a key ability of the brain, where context refers to information that characterizes the situation of an entity, e.g., place, time, emotional state, etc [66]. Context-awareness enables the brain to understand situations, react to new stimuli and make predictions from small datasets. Here, we examine a scenario where a robot receives spoken directions from a human being (driving input) and visually inspects a box (contextual input) and decides that it is safe to open the box if and only if the human being gives the direction to open and the box is not red in color (see Fig. 5 (a, b)).

This problem was implemented in simulation using T-SKONE that received a spoken command, which could be sent by a neuromorphic acoustic sensor [67], and a visual sensory input, which could be sent by a retinomorph sensor [68, 69]. As described in Methods, the spoken commands to not open (driving input ‘0’) and to open (driving input ‘1’) the box were encoded by a sinusoidal magnetic field excitation at 1.22 GHz and 1.85 GHz, respectively. Additionally, the color of the box being not red (modulatory input ‘0’) and being red (modulatory input ‘1’) led to T-SKONE being in Configuration I and II, respectively. The dynamical response of T-SKONE, which depends on the collective action of the two inputs, was simulated for all four combinations of inputs, and the output oscillations of $Sk5$ were analyzed (see Fig. 5 (c-f)). If the amplitude of oscillations of $Sk5$ along y were smaller than 1 nm, then the neuron had decided to open the box.

As shown in Fig. 5 (b, c-f), the neuron correctly decides to open the box, only under the conditions that it received a “go” command from the human collaborator (driving input ‘1’) and that the box is not red (modulatory input ‘0’). Critically, the solution is designed in such a way that, when the box is red in color (Configuration II), T-SKONE will not open the box regardless of the human command. However, when the box is not red in color (Configuration I), the decision to open the box depends upon the human command. The key reason is that in Configuration II the oscillations of $Sk5$ along y have considerable amplitude for both driving frequencies. However, in Configuration I the amplitude of oscillation remains large at 1.22 GHz but is smaller by a factor of 4 at 1.85 GHz from the amplitude seen in Configuration II. Thus, amplitude modulation makes T-SKONE useful for context-awareness.

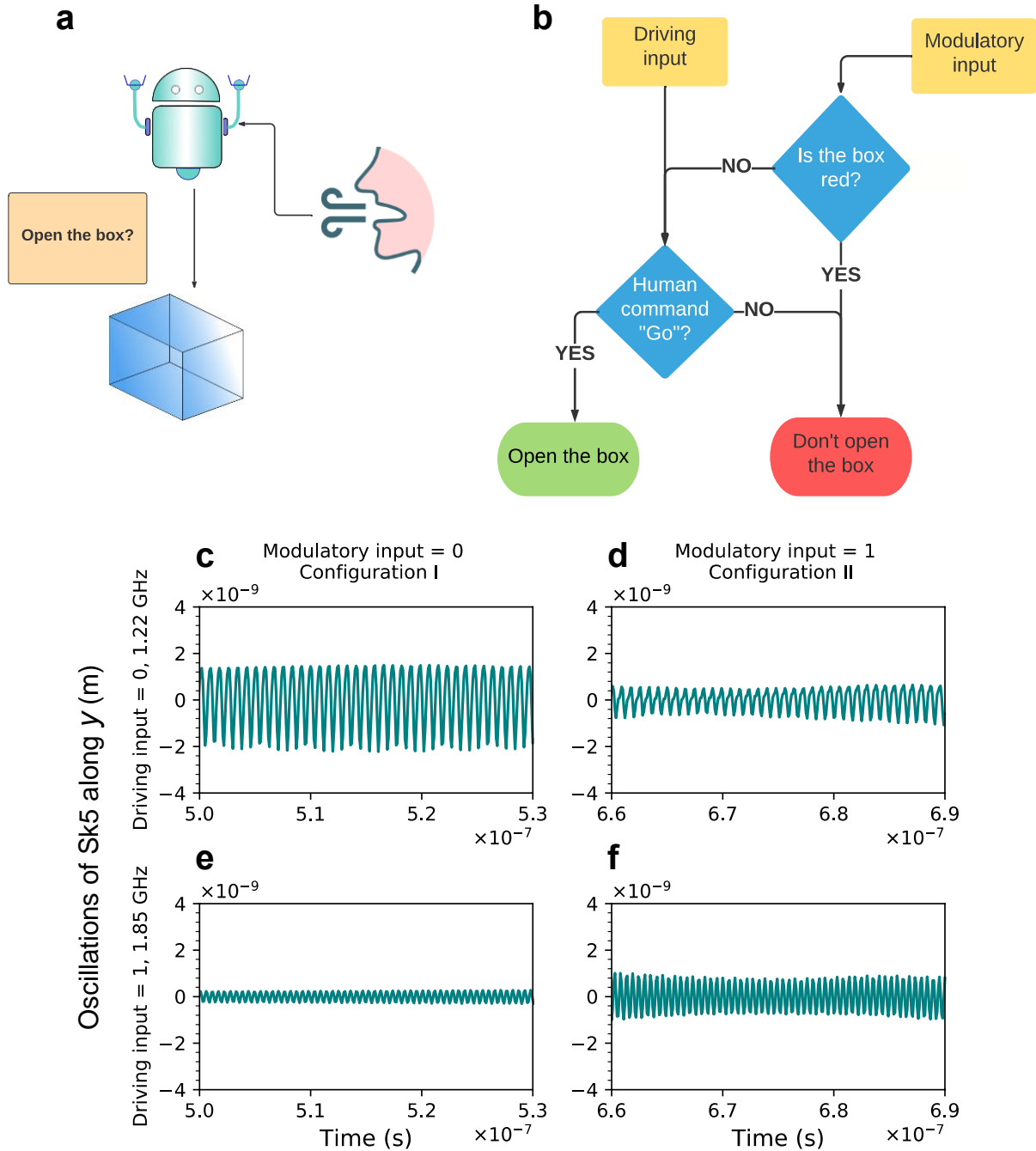


FIG. 5. Neuromorphic implementation of context-aware decision making. (a) Schematic of the decision-making task. A robot receives spoken directions from a human being, visually inspects a box and decides whether to open it. (b) Flowchart of the decision-making process. (c-f) Plot of the oscillations of *Sk5* along *y*. The combinations of driving and modulatory inputs are ('0', '0') in (c), ('0', '1') in (d), ('1', '0') in (e) and ('1', '1') in (f), respectively. Driving inputs '0' and '1' encode a sinusoidal excitation of frequency 1.22 GHz and 1.85 GHz, respectively. Modulatory inputs '0' and '1' lead to T-SKONE in Configuration I and II, respectively. (a,b) are created in Lucidchart [81].

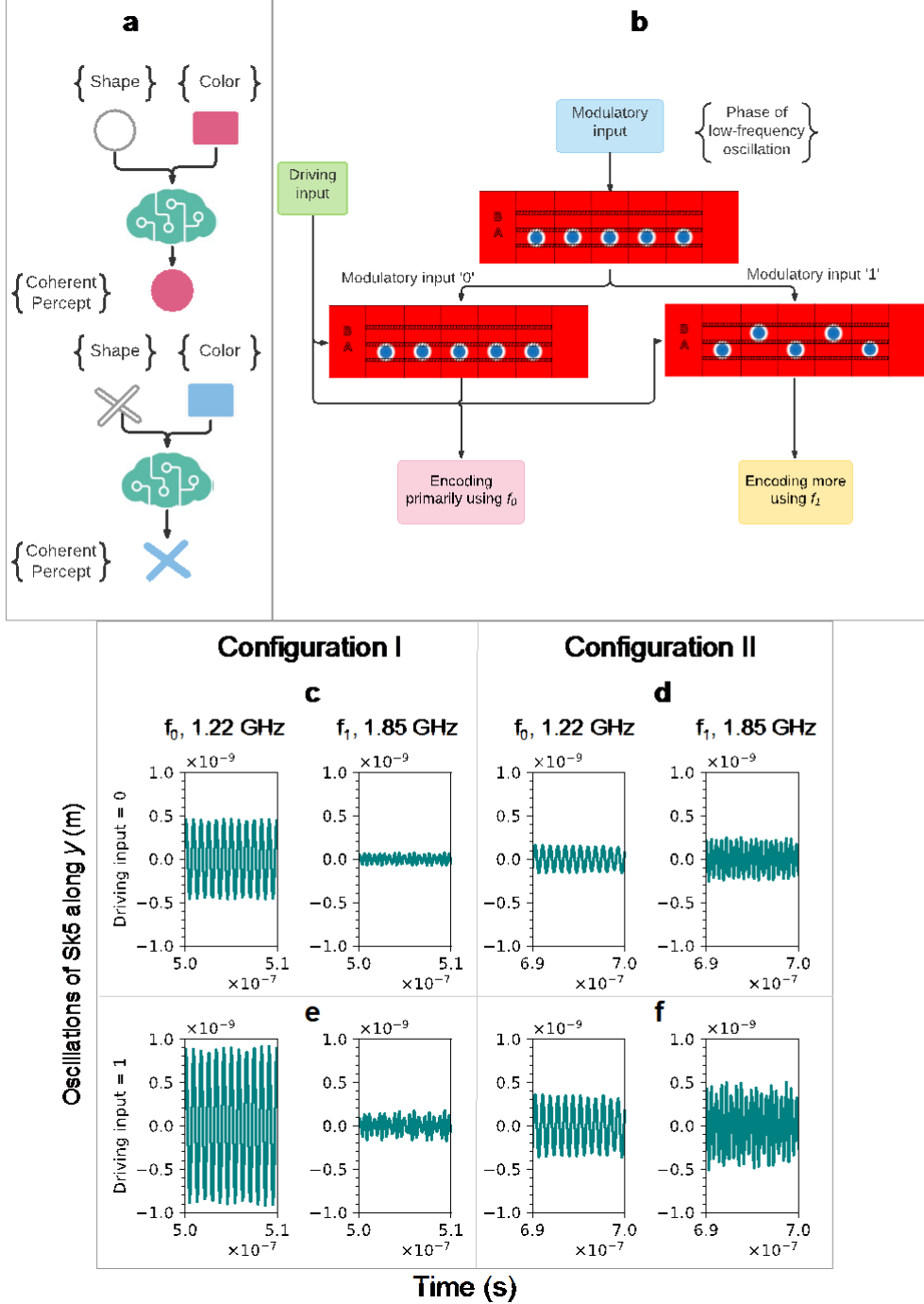


FIG. 6. Neuromorphic implementation of feature binding. (a) Schematic of the task. An advanced AI combines two features, shape and color, to form a coherent percept. (b) Flowchart of feature binding process. (c-f) Plot of the oscillations of Sk5 along y with the driving input as the sum of two sinusoidal magnetic fields of frequencies f_0 (1.22 GHz) and f_1 (1.85 GHz). ‘0’ is encoded by a magnetic field amplitude of $2.5 Oe$ and ‘1’ is encoded by an amplitude of $5.0 Oe$. Each subplot shows the frequency resolved output component for f_0 in the left column and for f_1 in the right column. The combinations of driving input with configuration shown are (‘0’, I) in (c), (‘0’, II) in (d), (‘1’, I) in (e) and (‘1’, II) in (f). (a, b) are created in Lucidchart [81].

Like context-awareness, feature binding is an advanced cognitive ability of the brain by which it combines different features of a perceived object that are processed in different regions of the brain to form a coherent perception of the object (see Fig. 6 (a)). Feature binding is a critical requirement of the brain’s ability to integrate inputs from multiple sensory streams and form a coherent internal picture of a complex and dynamic environment. Taking inspiration from the brain, here we implement feature binding based on synchrony and phase-coding. Therein, the phase of a low-frequency modulatory oscillation helps to bind the various features of an object by ensuring that different features of the same object are encoded at the same frequency, such that they can be correctly combined via synchronization.

In this setup, a network of ten T-SKONEs is shown two objects in sequence: a red circle and a blue cross. The two features of a perceived object, color and shape, are encoded in one bit and a 3×3 pixel array, respectively, and processed in parallel by different neural circuits. After processing, the network has to correctly combine the features, e.g., ‘red’ and ‘circle’, to obtain a coherent percept of the original object, i.e., ‘red circle’. The problem is simulated as described in Methods with the object features forming the driving input and the phase of a low-frequency oscillation ($0, \pi$) forming the modulatory input (see Fig. 6 (b)). The driving input is encoded by an oscillating magnetic field $H_{RF} = H_0(\sin(\omega_0 t) + \sin(\omega_1 t))$, where $\omega_i = 2\pi \times f_i$ and $f_0 = 1.22$ GHz and $f_1 = 1.85$ GHz. For the driving input ‘0’, $H_0 = 2.5$ Oe and for the driving input ‘1’, $H_0 = 5.0$ Oe. As the phase of the low-frequency oscillation changes every 100 ns between 0 and π , the modulatory input switches between ‘0’ and ‘1’ and all ten neurons in the network switch their configuration, thereby switching their frequencies of oscillation. Thus, objects perceived in different time windows are encoded at different frequencies.

Figure 6 (c-f) plot the encoding of driving inputs by a single T-SKONE for both configurations and demonstrates that the frequency basis used to encode a driving input markedly changes with change in the neuronal configuration. In Configuration I, the driving inputs are encoded primarily in f_0 (1.22 GHz), while in Configuration II, they are encoded to a greater extent in f_1 (1.85 GHz) than f_0 . This is because in Configuration I the oscillatory output of *Sk5* is larger for f_0 , while in Configuration II the output is larger for f_0 . As a result, when the first object is perceived, say at time t_I , all neurons are in Configuration I, and object features are encoded primarily at frequency f_0 . In contrast, when the second object is perceived, at time $t_{II} = t_I + 100$ ns, all neurons are in Configuration II, and the features are encoded with a greater component from frequency f_1 and a smaller component from f_0 . Thus, separate features of an object can be robustly and automatically combined in hardware via synchronization, implementing phase-coding enabled feature binding. Using additional circuitry to filter out the frequency component with a smaller amplitude will encode the first object purely at f_0 and the second object purely at f_1 , making the code more robust. Alternatively, the optimal selection of configurations to maximize the contrast between the frequency encodings for different objects will also enhance this robustness.

CONCLUSION

We have designed and validated the functions of a self-adaptive neuron utilizing a lattice of five coupled skyrmions and incorporated into it two advanced neuronal properties: oscillatory dynamics and neuromodulation. The neuron demonstrates a multi-frequent spectrum with four distinct modes whose amplitudes and frequencies are modified via lattice reconfiguration. Further, we have shown that the neuron displays bio-plausible dynamics including cross-frequency coupling and bursting as well as advanced cognitive processes such as context-awareness and feature binding. Our work is an important step towards the neuromorphic implementation of advanced cognition which can usher in the next wave of context-aware AI with high environmental adaptiveness and human interaction capabilities. The realization of this advanced AI requires more work, including the design of room-temperature stable insulating skyrmion materials and the integration of such neurons into large-scale neuromorphic architectures.

METHODS

Material parameters used for micromagnetic modeling of the TmIG/Pt system were taken from references [62] [70]: saturation magnetization $M_{sat} = 50 \times 10^3 \text{ A/m}$, exchange stiffness $A_{ex} = 0.8 \times 10^{-12} \text{ J/m}$, interfacial Dzyaloshinskii-Moriya constant $D_{ind} = 50 \times 10^{-6} \text{ J/m}^2$, Gilbert damping constant $\alpha = 0.02$, perpendicular magnetic anisotropy (PMA) $K_u = 1.8 \times 10^3 \text{ J/m}^3$ and $2.0 \times 10^3 \text{ J/m}^3$ for the reduced anisotropy regions (pinning sites) and normal regions, respectively. The neuron consists of five nanotracks of width of 180 nm (along x , coordinates defined in Fig. 1). There were two high-anisotropy track regions of length 56 nm (along y) alternating between three low-anisotropy pinning wells of length 12 nm (along y). The neuron was padded along x and y with unpatterned magnetic material to enhance skyrmion stability and closed boundary conditions were employed. In all simulations, a DC magnetic field of amplitude $H_{DC} = 240 \text{ Oe}$ was applied to the neuron in order to stabilize the skyrmions. The application of this DC field is required for skyrmion stability specifically in the TmIG/Pt system [62], but is not required for the neuron's design or functionality.

To calculate the FFT spectrum, the neuron was first excited with an external magnetic field $H_{RF} = H_0 \text{sinc}(\omega t)$ along x for 1 ns, with the amplitude of the magnetic field $H_0 = 40 \text{ Oe}$ and the cutoff frequency $\omega = 2\pi \times f$ where $f = 60 \text{ GHz}$. The field was applied to all nanotracks for 1 ns. The neuron was subsequently allowed to relax, and its dynamics during relaxation was examined and the trajectories of the skyrmion cores were calculated using the method described in [13].

To demonstrate Amplitude Modulation, T-SKONE was excited in all nanotracks with a sinusoidal magnetic field $H_{RF} = H_0 \sin(\omega t)$ along x with $H_0 = 10 \text{ Oe}$ and $\omega = 2\pi \times f$, at a range of driving frequencies f , and the oscillatory output was calculated. The oscillations of the skyrmion cores along x and y are taken to be the neuronal response.

To demonstrate cross-frequency coupling and bursting dynamics, the neuron was continuously excited by a sinusoidal magnetic field of 0.80 GHz in the first calculation and 1.85 GHz in the second calculation. Every 100 ns the neuron was switched in configuration between Configuration I & II. In other words, a modulatory input of 10 MHz was applied to periodically reconfigure the neuron. The amplitude of oscillation of Sk_2 along x was analyzed for the first calculation, and that of Sk_5 along x was analyzed for the second calculation. Reconfiguration was carried out using spin orbit torque applied by an electric current pulse of density 10^{11} A/m² and duration of 0.8 ns using a spin Hall angle of 0.02 corresponding to Pt.

In the implementation of context-awareness, the spoken human command was encoded in the driving input and the color of the box was encoded in the modulatory input which controlled the configuration of T-SKONE. The spoken command was frequency coded, i.e., the command to refrain from opening the box was encoded by a sinusoidal magnetic field of frequency 1.22 GHz and was labeled driving input ‘0’, whereas that to open the box was encoded at 1.85 GHz and labeled driving input ‘1’. The amplitude of the sinusoidal magnetic field was $10 Oe$. This driving input can be generated from the natural output of the acoustic sensor that is a frequency-selective oscillating voltage, by mapping the latter to higher frequencies. The contextual input from the retinomorph sensor is in the form of a digital voltage signal, where the absence of a voltage pulse signifies that the box is not red in color (labeled ‘0’) and the presence of a voltage pulse signifies that the box is red (labeled ‘1’). This voltage pulse gives rise to modulatory current inputs J_2 and J_4 , such that T-SKONE which is initially in Configuration I, upon receiving a voltage pulse switches to Configuration II. The dynamical response of T-SKONE was simulated for all four combinations of driving and modulatory inputs, and the output oscillations of Sk_5 were analyzed.

Feature binding was implemented with a network of T-SKONES. Information about the object features formed the driving input and the phase of a low-frequency oscillation formed the modulatory input. As the phase of the low-frequency oscillation changed with time, it controlled the configuration of all neurons in the network. Thus, the time at which an object was perceived determined the neuronal configurations, which in turn determined the frequencies at which the object features are encoded. The network received visual sensory input in the form of an oscillating magnetic field, which could be sent via a retinomorph sensor [68, 69]. The digital voltage output of the sensor could be converted into the oscillating magnetic field input by using a waveform generator. The network was designed to have two parts that process information in parallel. The first part (NC_{Color}) comprised a single T-SKONE and processed information about the color of the object, while the second part (NC_{Shape}) was composed of nine T-SKONES and processed information about the object shape. All visual information was amplitude coded and formed the driving input. The color ‘red’ was labeled driving input ‘0’ and the color ‘blue’ was labeled driving input ‘1’. The shape of the objects was in the form of a 3×3 pixel array, where ‘on’ and ‘off’ pixel states were labeled driving inputs ‘1’ and ‘0’, respectively. Each pixel output was sent to one T-

SKONE in NC_{Shape}. The ‘circle’ was represented with an input series {111101111}, while the ‘cross’ was represented with a series {101010101}. The driving input was encoded by an oscillating magnetic field $H_{RF} = H_0(\sin(\omega_0 t) + \sin(\omega_1 t))$, where $\omega_i = 2\pi \times f_i$ and $f_0 = 1.22$ GHz and $f_1 = 1.85$ GHz. For the driving input ‘0’, $H_0 = 2.5$ Oe and for the driving input ‘1’, $H_0 = 5.0$ Oe. The low-frequency oscillation was applied as periodic current pulses of frequency 10 MHz and was input as modulatory currents J_2 and J_4 , such that the neurons switched their configurations every 100 ns. The calculations as described above were carried out for one T-SKONE and the output of *Sk5* along *y* was analyzed. This oscillatory output of *Sk5* was filtered to obtain the two frequency components, i.e., $f_0 = 1.22$ GHz and $f_1 = 1.85$ GHz.

ACKNOWLEDGMENTS

The authors acknowledge funding from the National Science Foundation CAREER under award number 1940788, and computing resources from the Texas Advanced Computing Center (TACC) at the University of Texas at Austin (<http://www.tacc.utexas.edu>).

REFERENCES

- [1] I. Goodfellow, Y. Bengio and A. Courville, *Deep Learning*, The MIT Press, 2016.
- [2] Y. LeCun, Y. Bengio and G. Hinton, "Deep learning," *Nature*, vol. 521, p. 436–444, 2015.
- [3] S. Pouyanfar, S. Sadiq, Y. Yan, H. Tian, Y. Tao, M. P. Reyes, M.-L. Shyu, S.-C. Chen and S. S. Iyengar, "A Survey on Deep Learning: Algorithms, Techniques, and Applications," *ACM Computing Surveys* September, vol. 51, no. 5, p. 92, 2019.
- [4] DARPA, "DARPA Perspectives on AI," [Online]. Available: <https://www.darpa.mil/about-us/darpa-perspective-on-ai>.
- [5] B. Chatterjee, N. Cao, A. Raychowdhury and S. Sen, "Context-Aware Intelligence in Resource-Constrained IoT Nodes: Opportunities and Challenges," *IEEE Design & Test*, vol. 36, no. 2, pp. 7-40, 2019.
- [6] Cisco, "Cisco Global Cloud Index: Forecast and methodology 2016–2021 (Cisco, document 1513879861264127)," 2018.
- [7] P. A. Merolla, et al., "A million spiking-neuron integrated circuit with a scalable communication network and interface," *Science*, vol. 345, no. 6197, pp. 668-673, 2014.
- [8] F. C. Bauer, D. R. Muir and G. Indiveri, "Real-Time Ultra-Low Power ECG Anomaly Detection Using an Event-Driven Neuromorphic Processor," *IEEE Transactions on Biomedical Circuits and Systems*, vol. 13, no. 6, pp. 1575 - 1582, 2019.

- [9] B. Rajendran, A. Sebastian, M. Schmuker, N. Srinivasa and E. Eleftheriou, "Low-Power Neuromorphic Hardware for Signal Processing Applications: A Review of Architectural and System-Level Design Approaches," *IEEE Signal Processing Magazine*, vol. 36, no. 6, pp. 97 - 110, 2019.
- [10] J. Grollier, D. Querlioz, K. Y. Camsari, K. Everschor-Sitte, S. Fukami and M. D. Stiles, "Neuromorphic spintronics," *Nature Electronics*, vol. 3, p. 360–370, 2020.
- [11] S. Singh, A. Sarma, N. Jao, A. Pattnaik, S. Lu, K. Yang, A. Sengupta, V. Narayanan and C. R. Das, "NEBULA: A Neuromorphic Spin-Based Ultra-Low Power Architecture for SNNs and ANNs," in *ACM/IEEE 47th Annual International Symposium on Computer Architecture (ISCA)*, Valencia, Spain, 2020.
- [12] W. Kang, Y. Huang, X. Zhang, Y. Zhou and W. Zhao, "Skyrmion-Electronics: An Overview and Outlook," *Proceedings of the IEEE*, vol. 104, no. 10, pp. 2040 - 2061, 2016.
- [13] J. Kim, J. Yang, Y.-J. Cho, B. Kim and S.-K. Kim, "Coupled gyration modes in onedimensional skyrmion arrays in thin-film nanostrips as new type of information carrier," *Scientific Reports*, vol. 7, p. 45185, 2017.
- [14] M. I. Trukhanova and P. Andreev, "A quantum hydrodynamical model of skyrmions with electrical dipole moments and novel magneto-electric skyrmion Hall effect," *Progress of Theoretical and Experimental Physics*, vol. 2020, no. 4, p. 043I01, 2020.
- [15] M. Davies et al., "Loihi: A Neuromorphic Manycore Processor with On-Chip Learning," in *IEEE Micro*, 2018.
- [16] A. Sengupta, A. Banerjee and K. Roy, "Hybrid Spintronic-CMOS Spiking Neural Network with On-Chip Learning: Devices, Circuits, and Systems," *Physical Review Applied*, vol. 6, p. 064003, 2016.
- [17] E. Marder, "Dynamic Modulation of Neurons and Networks," in *Advances in Neural Information Processing Systems 6 (NIPS)*, 1993.
- [18] R. A. Silver, "Neuronal arithmetic," *Nature Reviews*, vol. 11, p. 474, 2010.
- [19] M. A. Whittington, R. D. Traub and N. E. Adams, "A future for neuronal oscillation research," *Brain and Neuroscience Advances*, vol. 2, pp. 1-6, 2018.
- [20] F. Nadim and D. Bucher, "Neuromodulation of Neurons and Synapses," *Curr Opin Neurobiol.*, vol. 0, p. 48–56, 2014.
- [21] M. Siegel, A. K. Engel and T. H. Donner, "Cortical network dynamics of perceptual decision-making in the human brain," *Frontiers in Human Neuroscience*, vol. 5, p. 21, 2011.
- [22] R. F. Helfrich and R. T. Knight, "Oscillatory Dynamics of Prefrontal Cognitive Control," *Trends in Cognitive Sciences*, vol. 20, no. 12, p. 916, 2016.
- [23] C. Tallon-Baudry and O. Bertrand, "Oscillatory gamma activity in humans and its role in object representation," *Trends in Cognitive Sciences*, vol. 3, no. 4, p. 151, 1999.

- [24] W. Singer and C. M. Gray, "Visual feature integration and the temporal correlation hypothesis," *Annu. Rev. Neurosci.*, vol. 18, p. 555, 1995.
- [25] S. Karakas, C. Basar-Eroglu, C. Ozesmi, H. Kafadar and O. U. Erzen, "Gamma response of the brain: a multifunctional oscillation that represents bottom-up with top-down processing," *International Journal of Psychophysiology*, vol. 39, pp. 137-150, 2001.
- [26] A. Wutz, D. Melcher and J. Samaha, "Frequency modulation of neural oscillations according to visual task demands," *PNAS*, vol. 115, no. 6, p. 1346–1351, 2018.
- [27] B. Voytek, R. T. Canolty, A. Shestyk, N. E. Crone, J. Parvizi and R. T. Knight, "Shifts in gamma phase–amplitude coupling frequency from theta to alpha over posterior cortex during visual tasks," *Frontiers in Human Neuroscience*, vol. 4, p. 191, 2010.
- [28] G. Indiveri, "Modeling Selective Attention Using a Neuromorphic Analog VLSI Device," *Neural Computation*, vol. 12, p. 2857–2880, 2000.
- [29] L. Gao, P.-Y. Chen and S. Yu, "NbOx based oscillation neuron for neuromorphic computing," *Appl. Phys. Lett.*, vol. 111, p. 103503, 2017.
- [30] T. Jackson, S. Pagliarini and L. Pileggi, "An Oscillatory Neural Network with Programmable Resistive Synapses," in *28 nm CMOS, IEEE International Conference on Rebooting Computing*, 2018.
- [31] J. Torrejon, et al., "Neuromorphic computing with nanoscale spintronic oscillators," *Nature*, vol. 547, p. 428, 2017.
- [32] M. Romera, et al., "Vowel recognition with four coupled spin-torque nano-oscillators," *Nature*, vol. 563, p. 230, 2018.
- [33] M. A. Azam, D. Bhattacharya, D. Querlioz and J. Atulasimha, "Resonate and fire neuron with fixed magnetic skyrmions," *Journal of Applied Physics*, vol. 124, no. 152122, 2018.
- [34] A. J. Watrous, J. Fell, A. D. Ekstrom and N. Axmacher, "More than spikes: common oscillatory mechanisms for content specific neural representations during perception and memory," *Current Opinion in Neurobiology*, vol. 31, pp. 33-39, 2015.
- [35] S. Li, et al., "Magnetic skyrmion-based artificial neuron device," *Nanotechnology*, vol. 28, no. 31LT01, 2017.
- [36] X. Chen, et al., "A compact skyrmionic leaky–integrate–fire spiking neuron device," *Nanoscale*, vol. 10, p. 6139, 2018.
- [37] M.-C. Chen, A. Sengupta and K. Roy, "Magnetic Skyrmion as a Spintronic Deep Learning Spiking Neuron Processor," *IEEE Transactions on Magnetics*, vol. 54, p. 1500207, 2018.
- [38] N. Hakim and E. K. Vogel, "Phase-coding memories in mind," *PLOS Biology*, vol. 16, no. 8, p. 1, 2018.
- [39] A. J. Watrous, J. Miller, S. E. Qasim, I. Fried and J. Jacobs, "Phase-tuned neuronal firing encodes human contextual representations for navigational goals," *eLife*, vol. 7, p. e32554, 2018.

- [40] M. Volgushev, M. Chistiakova and W. Singer, "Modification of discharge patterns of neocortical neurons by induced oscillations of the membrane potential," *Neuroscience*, vol. 83, no. 1, pp. 15-25, 1998.
- [41] P. Fries, D. Nikolić and W. Singer, "The gamma cycle," *Trends in Neuroscience*, vol. 30, no. 7, pp. 309-316, 2007.
- [42] M. X. Cohen, "Fluctuations in oscillation frequency control spike timing and coordinate neural networks," *Journal of Neuroscience*, vol. 34, no. 27, p. 8988–8998, 2014.
- [43] C. Kayser, R. A. Ince and S. Panzeri, "Analysis of slow (theta) oscillations as a potential temporal reference frame for information coding in sensory cortices," *PLoS Computational Biology*, vol. 8, no. 10, p. e1002717, 2012.
- [44] P. M. A. Milner, "A model for visual shape recognition," *Psychological Review*, vol. 81, no. 6, pp. 521-535, 1974.
- [45] S. Grossberg , "Adaptive pattern classification and universal recoding: I. Parallel development and coding of neural feature detectors," *Biological Cybernetics*, vol. 23, p. 121–134, 1976.
- [46] C. von der Malsburg, "The correlation theory of brain function," Internal Report. Dept. of Neurobiology, Max-Planck-Institute for Biophysical Chemistry, Göttingen, Germany., 1981.
- [47] C. M. Gray and W. Singer, "Stimulus-specific neuronal oscillations in orientation columns of cat visual cortex," *Proc. Natl. Acad. Sci. USA*, vol. 86, pp. 1698-1702, 1989.
- [48] C. M. Gray, P. König, A. K. Engel and W. Singer , "Oscillatory responses in cat visual cortex exhibit inter-columnar synchronization which reflects global stimulus properties," *Nature*, vol. 338, pp. 334-37, 1989.
- [49] A. A. Abdellatif, A. Mohamed, C. F. Chiasserini, M. Tlili and A. Erbad, "Edge Computing for Smart Health: Context-Aware Approaches, Opportunities, and Challenges," *IEEE Network*, vol. 33, no. 3, pp. 196-203, 2019.
- [50] R. Fernandez-Rojas, A. Perry, H. Singh, B. Campbell, S. Elsayed, R. Hunjet and H. A. Abbass, "Contextual Awareness in Human-Advanced-Vehicle Systems: A Survey," *IEEE Access*, vol. 7, pp. 33304-33328, 2019.
- [51] F. Belkadi, M. A. Dhuieb, J. V. Aguado, F. Laroche, A. Bernard and F. Chinesta, "Intelligent assistant system as a context-aware decision-making support for the workers of the future," *Computers & Industrial Engineering*, vol. 139, p. 105732, 2020.
- [52] E. Ceolini, C. Frenkel, S. B. Shrestha, G. Taverni, L. Khacef, M. Payvand and E. Donati, "Hand-Gesture Recognition Based on EMG and Event-Based Camera Sensor Fusion: A Benchmark in Neuromorphic Computing," *Frontiers in Neuroscience*, vol. 14, p. 637, 2020.
- [53] J. Fayyad , M. A. Jaradat, D. Gruyer and H. Najjaran, "Deep Learning Sensor Fusion for Autonomous Vehicle Perception and Localization: A Review," *Sensors*, vol. 20, no. 15, p. 4220, 2020.

- [54] M. Muzammal, R. Talat, A. H. Sodhro and S. Pirbhulal, "A multi-sensor data fusion enabled ensemble approach for medical data from body sensor networks," *Information Fusion*, vol. 53, pp. 155-164, 2020.
- [55] R. R. Shamshiri, I. Bojic, E. van Henten, S. K. Balasundram, V. Dworak, M. Sultan and C. Weltzien, "Model-based evaluation of greenhouse microclimate using IoT-Sensor data fusion for energy efficient crop production," *Journal of Cleaner Production*, vol. 263, p. 121303, 2020.
- [56] P. G. Schyns, G. Thut and J. Gross, "Cracking the Code of Oscillatory Activity," *PLoS Biology*, vol. 9, no. 5, p. e1001064, 2011.
- [57] A. Cortese, B. De Martino and M. Kawato, "The neural and cognitive architecture for learning from a small sample," *Current Opinion in Neurobiology*, vol. 55, pp. 33-141, 2019.
- [58] J. Wells, J. H. Lee, R. Mansell, R. P. Cowburn and O. Kazakova, "Controlled manipulation of domain walls in ultra-thin CoFeB nanodevices," *Journal of Magnetism and Magnetic Materials*, vol. 400, pp. 219-224, 2016.
- [59] K. Moon, B. Chun, W. Kim and C. Hwang, "Control of spin-wave refraction using arrays of skyrmions," *Physical Review Applied*, vol. 6, no. 6, p. 064027, 2016.
- [60] M. Mochizuki, "Spin-Wave Modes and Their Intense Excitation Effects in Skyrmion Crystals," *Phys. Rev. Lett.*, vol. 108, p. 017601, 2012.
- [61] Y. Onose, Y. Okamura, S. Seki, S. Ishiwata and Y. Tokura, "Observation of Magnetic Excitations of Skyrmion Crystal in a Helimagnetic Insulator Cu₂OSeO₃," *Phys. Rev. Lett.*, vol. 109, p. 037603, 2012.
- [62] Q. Shao, Y. Liu, G. Yu, S. Kim, X. Che, C. Tang, Q. He, Y. Tserkovnyak, J. Shi and K. Wang, "Topological Hall effect at above room temperature in heterostructures composed of a magnetic insulator and a heavy metal," *Nature Electronics*, vol. 2, no. 5, pp. 182-186., 2019.
- [63] S. Vélez, J. Schaab, M. Wörnle, M. Müller, E. Gradauskaite, P. Welter, C. Gutfleider, C. Nistor, C. Degen, M. Trassin and M. Fiebig, "High-speed domain wall racetracks in a magnetic insulator," *Nature communications*, vol. 10, no. 1, pp. 1-8, 2019.
- [64] C. Avci, E. Rosenberg, L. Caretta, F. Büttner, M. Mann, C. Marcus, D. Bono, C. Ross and G. Beach, "Interface-driven chiral magnetism and current-driven domain walls in insulating magnetic garnets," *Nature nanotechnology*, vol. 14, no. 6, pp. 561-5, 2019.
- [65] A. Vansteenkiste, J. Leliaert, M. Dvornik, M. Helsen, F. Garcia-Sanchez and B. Van Waeyenberge, "The design and verification of MuMax3," *AIP advances*, vol. 4, no. 10, p. 107133, 2014.
- [66] A. K. Dey, D. Salber, G. D. Abowd and M. Futakawa, "Providing Architectural Support for Building Context-Aware Application," College of Computing, Georgia Institute of Technology, 2000.

- [67] J. Jang, J. Lee, S. Woo, D. J. Sly, L. J. Campbell, J.-H. Cho, S. J. O’Leary, M.-H. Park, S. Han, J.-W. Choi, J. H. Jang and H. Choi, "A microelectromechanical system artificial basilar membrane based on a piezoelectric cantilever array and its characterization using an animal model," *Scientific Reports*, vol. 5, p. 12447, 2015.
- [68] P. Lichtsteiner, T. Delbruck and J. Kramer, "Improved ON/OFF temporally differentiating address-event imager," in *Proceedings of the 11th IEEE International Conference on Electronics, Circuits and Systems (ICECS)*, Tel-Aviv, 2004.
- [69] A. Vanarse, A. Osseiran and A. Rassau, "A Review of Current Neuromorphic Approaches for Vision, Auditory, and Olfactory Sensors," *Frontiers in Neuroscience*, vol. 10, p. 115, 2016.
- [70] O. Ciubotariu, A. Semisalova, K. Lenz and M. Albrecht, "Strain-induced perpendicular magnetic anisotropy and Gilbert damping of Tm₃Fe₅O₁₂ thin films," *Scientific reports*, vol. 9, no. 1, pp. 1-8, 2019.
- [71] M. E. Hasselmo and M. Sarter, "Modes and Models of Forebrain Cholinergic Neuromodulation of Cognition," *Neuropsychopharmacology Reviews*, vol. 36, p. 52–73, 2011.
- [72] J. Kim, J. Yang, Y. Cho, B. Kim and S. Kim, "Coupled gyration modes in one-dimensional skyrmion arrays in thin-film nanostrips as new type of information carrier," *Scientific reports*, vol. 7, p. 45185, 2017.
- [73] S. Angra and S. Ahuja, "Machine learning and its applications: A review," in *2017 International Conference on Big Data Analytics and Computational Intelligence (ICBDAC)*, Chirala, India, 2017.
- [74] U. Alegre, J. C. Augusto and T. Clark, "Engineering context-aware systems and applications: A survey," *Journal of Systems and Software*, vol. 117, pp. 55-83, 2016.
- [75] W. F. Lawless, R. Mittu, D. Sofge and L. Hiatt, "Artificial Intelligence, Autonomy, and Human-Machine Teams: Interdependence, Context, and Explainable AI.," *AI Magazine*, vol. 40, no. 3, pp. 5-13, 2019.
- [76] D. Senkowski, T. R. Schneider, J. J. Foxe and A. K. Engel, "Crossmodal binding through neural coherence: implications for multisensory processing," *Trends in Neurosciences*, vol. 31, no. 8, pp. 401-409, 2008.
- [77] A. K. Engel, P. Fries, P. Konig, M. Brecht and W. Singer, "Temporal Binding, Binocular Rivalry, and Consciousness," *Consciousness and Cognition*, vol. 8, no. 2, pp. 128-151, 1999.
- [78] W. Singer, "Neuronal synchrony: A versatile code for the definition of relations?," *Neuron*, vol. 24, pp. 49-65, 1999.
- [79] R. Eckhorn, R. Bauer, W. Jordan, M. Brosch, W. Kruse, M. Munk and H. J. Reitboeck, "Coherent Oscillations: A Mechanism of Feature Linking in the Visual Cortex?," *Biological Cybernetics*, vol. 60, pp. 121-130, 1988.

- [80] C. Kayser, R. A. A. Ince and S. Panzeri, "Analysis of Slow (Theta) Oscillations as a Potential Temporal Reference Frame for Information Coding in Sensory Cortices," *PLoS Computational Biology*, vol. 8, no. 10, p. e1002717, 2012.
- [81] Lucidchart. [Online]. Available: <https://www.lucidchart.com/>.